Resistance Resonance Effects through Magnetic Edge States

A. Nogaret and S. J. Bending
Department of Physics, University of Bath, Bath BA2 7AY, United Kingdom

M. Henini
School of Physics and Astronomy, University of Nottingham, Nottingham NG7 2RD, United Kingdom
(Received 3 September 1999)

We report on the magnetoresistance of a two-dimensional electron gas subjected to an abrupt magnetic field gradient arising from a ferromagnetic stripe fabricated at its surface. A sharp resistance resonance effect is observed at B_p due to the formation of two types of magnetic edge states that drift in opposite directions perpendicular to the magnetic field gradient for $B < B_p$ and $B > B_p$. A semiclassical drift-diffusion model gives a good description of the effects of the magnetic confinement on both the diagonal and off-diagonal components of the resistivity tensor.

PACS numbers: 73.50.Jt, 72.15.Gd

High mobility two-dimensional electron gases (2DEG) with mean free paths in excess of several microns allow the effects of a small potential modulation to dominate in the resistivity [1,2]. Recent advances in nanofabrication allow microstructured magnetic potentials to be applied to ballistic electron systems. Microscopic magnetic barriers with amplitude of several thousand gauss were formed in nonplanar devices [3] or by gating a 2DEG with micromagnets [4–6] or superconductors [7]. The influence of a magnetic modulation on ballistic electrons was demonstrated experimentally via commensurability effects between the classical cyclotron diameter and the period of a magnetic superlattice [4,5,7]. These findings have since been generalized to 2D superlattices [8] and composite fermion systems [9]. An interesting situation arises when the sign of the magnetic modulation and therefore the Lorentz force alternates. In addition to conferring a drift to the cyclotron guiding center, the magnetic gradient confines electrons about the boundary line between two regions of opposite magnetic field [4,10]. Recent theoretical developments have focused on the energy spectrum and the physical properties of electrons quantum mechanically confined in this way [11]. Sharp resonances in the magnetization [12] and conductance [13] of a magnetic antidot have been associated with the formation of novel magnetic edge states circulating clockwise and anticlockwise about the antidot.

In this Letter, we investigate the magnetoresistance of 2D electrons confined by a transverse magnetic field gradient. A sharp peak is observed when the applied magnetic field cancels the modulation field. On either side of this peak, transport is controlled by one of the two magnetic edge states predicted in Refs. [12] and [13]. The effects of varying the magnetic gradient and the electron density confirm this picture. The dependencies of R_{xx} and R_{xy} are both modeled within a straightforward drift-diffusion theory. Our data show that in the presence of a strongly inhomogeneous current distribution the Hall resistance is *not* proportional to the magnetic field averaged over the Hall junction.

The experiments were performed on a standard GaAs/$Al_{0.3}Ga_{0.7}As$ heterojunction with electron density $n_s = 1.94 \times 10^{15}$ m^{-2}, and mean free path $l \sim 4.5$ μm at 4.2 K. Optical lithography and wet chemical etching were used to define the Hall devices as shown in Fig. 1(a). A narrow ferromagnetic stripe fabricated above the center of the electron channel imposes a magnetic step along the y direction. Several devices with 32 μm long and $d = 500$ nm wide stripes of iron or nickel have been prepared by electron beam lithography and lift-off techniques.

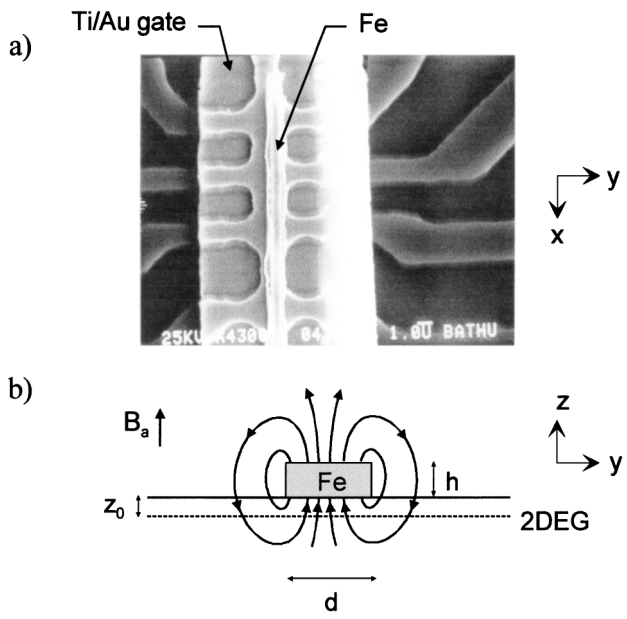

FIG. 1. (a) Hall device with a Fe stripe fabricated above its 2 μm wide channel. A Ti/Au gate overlaps the whole channel area. (b) Schematic cross section of the high mobility channel showing the structural parameters: $d = 500$ nm, $z_0 = 80$ nm, $h = 200$ nm.

In order to minimize averaging over regions unperturbed by the magnetic modulation, we chose a $2a = 2\ \mu$m wide 2DEG channel comparable in size to the cyclotron diameter in a field of 0.1 T ($2R_c \sim 1.5\ \mu$m). Finally, the whole channel area including the stripe was covered with a Ti/Au gate to achieve a uniform differential thermal contraction coefficient between metal layers and GaAs over the active area of the sample. Since the coefficients for Ti/Au and Fe (or Ni) are nearly identical [14], we expect no *local* piezoelectric modulation to build up underneath the stripe when the sample is cooled down [4,5,7].

Our samples were mounted inside a superconducting solenoid allowing a homogeneous magnetic field B_a to be applied normal to the 2DEG. The magnetization of a thin iron film on GaAs is known to be strongly uniaxial along the $\langle 011 \rangle$ direction within its plane [15]. This direction corresponds to the long side of the stripe and is also the easy magnetization axis with respect to shape anisotropy [6]. Hence as the external magnetic field is increased, the magnetization, initially along the x axis, rotates to align with the z axis. Only the z component of the stray fields is responsible for the magnetic modulation and the 2D electrons will experience a positive effective magnetic field underneath the stripe and negative elsewhere as sketched in Fig. 1(b). Abrupt variations in the magnetic field profile are realized by choosing a stripe width ($d = 500$ nm) large compared to the depth of the 2DEG beneath the surface ($z_0 = 80$ nm) [16]. The devices were cooled to 4.2 K in zero external magnetic field. The magnetic field was then ramped up to $+1$ T and subsequently cycled between $+1$ T and -1 T without interruption through zero. The results shown below have been corrected for a 4 mT offset between sweep up and sweep down that arises due to the remanence of the solenoid as established in a structure without a magnetic stripe.

The magnetoresistance along an iron stripe is plotted in Fig. 2 for four values of gate bias. We used a 1 μA dc injection current and measured the corresponding voltage drop across probes set 16 μm apart. The trace at zero gate bias exhibits a sharp peak at $B_p = 32$ mT independent of the direction of the applied magnetic field. As B_a further increases, the magnetoresistance goes through a minimum at 180 mT before rising again. From the linear part of the Hall resistance (see below), we find that gate biases in the range -0.6 to $+0.5$ V change the electron density between 1.8 and 2.2×10^{11} cm^{-2}. Surprisingly, despite this large variation, the peak position remains the same within $\pm 2\%$ suggesting that the kinetics of Fermi electrons play no role. In the inset in Fig. 2, we now compare the low field magnetoresistance along both iron and nickel stripes. The effect of replacing iron by nickel scales the whole structure in R_{xx} down in magnetic field and the magnetoresistance peak with nickel is now at $B_p = 13$ mT. Iron has a saturation magnetization at 1.74 T compared to 0.51 T for nickel [17] and, assuming the magnetization of the iron and nickel stripes has the same angular dependence on the applied magnetic field, the ratio of their modulation strength is simply [16] $1.74/0.51 \sim 3.4$. The correspondence with the ratio of the experimental peak positions, $32/13 \sim 2.5$, is sufficiently good that we interpret the peak position to be determined by the strength of the magnetic modulation only. The asymmetric peak structure in Fig. 2 reflects a slight displacement of the stripe from the center of the channel. This is clearly demonstrated in the lowest curve of the main panel in Fig. 2 where the effect of switching to probes connected to the opposite side of the channel results in a reflection of the peak line shape about the y axis. The inset in Fig. 2 also shows a small hysteresis in R_{xx}. As the gate bias decreases below -0.3 V, a broad shoulder emerges from the positive magnetoresistance background around ± 350 mT. This background is drastically reduced by a fourfold reduction in the Hall bar aspect ratio which suggests its origin is scattering at diffuse channel boundaries; see the bottom curve in Fig. 2. We note the onset of Shubnikov–de Haas oscillations near 0.7 T at a gate bias of $+0.5$ V.

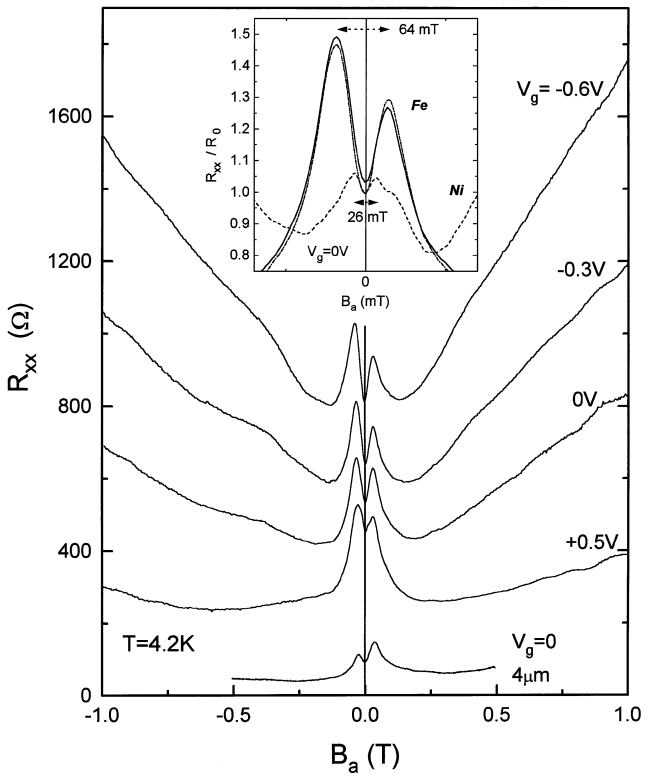

FIG. 2. The magnetoresistance of the Fe device measured at various gate biases between probes 16 μm apart. The bottom curve is measured using probes 4 μm apart on the opposite side of the channel. Inset: the normalized magnetoresistance of Ni and Fe (full line: sweep up; dash-dotted line: sweep down) devices.

The Hall resistance curves shown in the inset in Fig. 3 also exhibit a small but clear hysteresis consistent with the $\sim$5 mT wide hysteresis of iron films on (001) GaAs [15]. For $B_a < 200$ mT, R_{xy} is strongly nonlinear while, at higher fields, it tends towards the usual unperturbed Hall

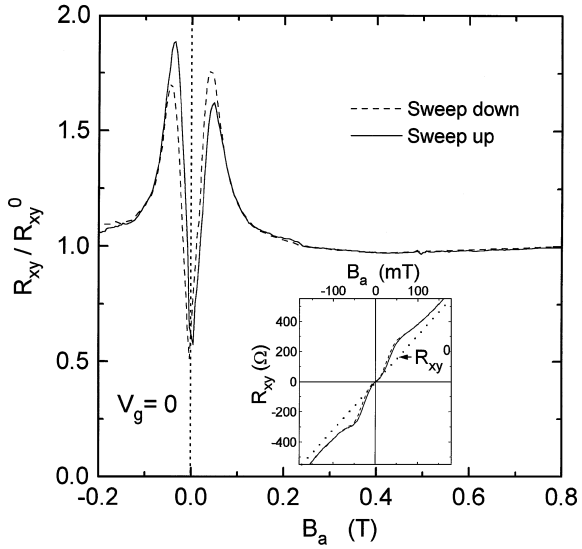

FIG. 3. The Hall resistance R_{xy}, in the presence of the magnetic modulation normalized by the unperturbed Hall resistance $R_{xy}^0 = B_a/en_s$. The inset shows the raw Hall data.

resistance R_{xy}^0. This asymptotic behavior extrapolates to the origin (dotted line in the inset in Fig. 3) and we directly extract the electron density n_s from this slope. The main plot in Fig. 3 shows the quantity R_{xy}/R_{xy}^0 which has several features reminiscent of the magnetoresistance in Fig. 2: (i) a value at $B_a = 0$ that is close to that of the normalized magnetoresistance $R_{xx}/R_{xx}(B_a = 0)$, (ii) a similar peak at ~38 mT, and (iii) a second (weak) minimum around 400 mT.

We have calculated the resistivity tensor for our system along the lines of Beenakker in Ref. [1]. A gradient of magnetic field along y causes an electron to drift along x with an average velocity v_d. This enhances the diffusivity along x by $\delta D_{xx} = \langle v_d^2 \rangle \tau$ [1,2], where τ is the classical scattering time and the average is over the Fermi surface. Using Einstein's equation $\rho = (h/4\pi m^* e^2)\mathbf{D}^{-1}$ to find the resistivity components:

$$\frac{\rho_{xx}}{\rho_0} = 1 - \frac{2\langle v_d^2 \rangle / v_F^2}{1 + 2\langle v_d^2 \rangle / v_F^2} \tag{1}$$

and

$$\rho_{xy} = \frac{B_a}{en_s} \frac{\rho_{xx}}{\rho_0}, \tag{2}$$

where $\rho_0 = h/(k_F l e^2)$ is the zero field resistivity, $k_F = \sqrt{2\pi n_s}$ and $v_F = \hbar k_F / m^*$ are the Fermi wave vector and Fermi velocity, respectively, and m^* is the effective mass in GaAs. The magnetic profile produced by a rectangular stripe was solved in Ref. [16] and is shown in the right inset in Fig. 4 for the structure of Fig. 1(b) with the saturation magnetization of iron. In order to keep the derivation of v_d analytic while retaining the essential physics, we approximate the exact profile by the mean magnetic field below the stripe and away from the stripe. This new rectangular profile exhibits two levels at $B_1^0 = -60$ mT and $B_2^0 = 280$ mT as seen in the right inset in Fig. 4. The superscript here denotes $B_a = 0$. As long as $|B_a| < |B_1^0|$ the magnetic field changes sign across the step boundary. An electron crossing this boundary at an angle $\phi < \phi_{\max}$ is trapped in a snakelike orbit similar to the one shown in the left inset in Fig. 4. $\phi_{\max}$ represents the maximum angle beyond which an electron reaches the channel boundary [10]. Increasing the magnetic field decreases the negative step height to $B_1 = B_a + B_1^0$. As a consequence the number of trapped orbits decreases and so does $\phi_{\max}$. The drift velocity is given by $v_d = v_F(\sin\phi/\phi)$ and after integration over the Fermi surface we obtain

$$\langle v_d^2 \rangle = \frac{v_F^2}{\pi} \int_0^{\phi_{\max}} d\phi \left(\frac{\sin\phi}{\phi} \right)^2, \quad \text{where } \phi_{\max} = \min(\phi_1, \phi_2) \tag{3}$$

with

$$\phi_1 = \begin{cases} \cos^{-1}[1 - (a - d/2)/R_{c1}], & \text{if } 2R_{c1} > a - d/2, \\ \pi, & \text{otherwise} \end{cases}$$

and

$$\phi_2 = \begin{cases} \cos^{-1}(1 - d/R_{c2}), & \text{if } 2R_{c2} > d, \\ \pi, & \text{otherwise.} \end{cases}$$

When $B_a > |B_1^0|$, the classical trajectories across the magnetic step are cycloidlike as shown in the central inset in Fig. 4. Differences in cyclotron radius across the step induce a drift in the opposite direction to the snakelike orbits. After calculating v_d for the cycloid orbits we obtain

$$\langle v_d^2 \rangle = \frac{v_F^2}{\pi} \int_{\phi_2'}^{\phi_1} d\phi \left(\frac{B_2 - B_1}{\pi B_1 + \phi(B_2 - B_1)} \sin\phi \right)^2 \tag{4}$$

where $\phi_2' = \pi - \phi_2$.

We model the stripes as *ideal* ferromagnets so that the magnetic modulation immediately reaches its maximum at vanishingly small B_a. The theoretical magnetoresistance [Eq. (1)] is shown in Fig. 4.

The sharp magnetoresistance peak in Fig. 4 marks the cancellation of the negative modulation step by the applied magnetic field, i.e., $B_p + B_1^0 = 0$. The positive magnetic field barrier below the stripe deflects electrons towards the surrounding regions where the total field is zero, hence the zero field resistivity at the peak. Our model probably overestimates the peak position because the magnetization saturates at 50 mT, well above the measured B_p. Figure 2 shows a fall in the zero field resistance relative to the peak when the electron density decreases. This result may seem paradoxical given evidence elsewhere for a simultaneous reduction in mobility. In fact, the fraction of snakelike

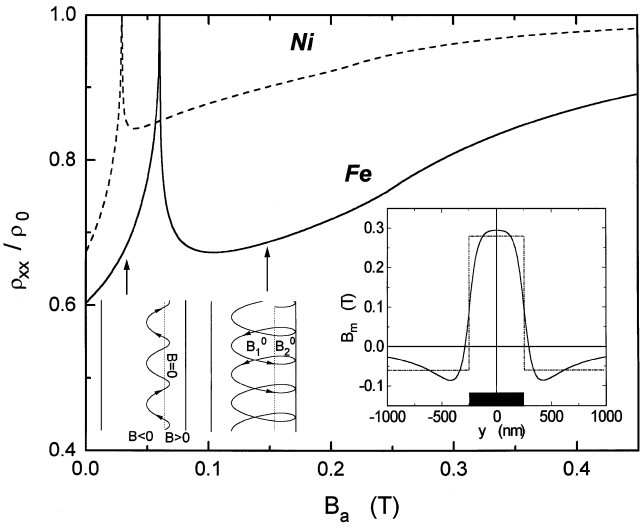

FIG. 4. Normalized magnetoresistance calculated for both iron and nickel devices (see text). Snake- and cycloidlike magnetic edge states are illustrated in the left and central insets at magnetic fields of 0.05 and 0.15 T, respectively. In these insets, the dashed line represents the step edge at $y = -250$ nm; the vertical sidelines represent the left boundary and the center of the channel, respectively. The exact magnetic profile underneath a Fe stripe is shown in the right inset. The rectangular approximation used to calculate the resistivity is plotted with a dash-dotted line.

states increases as a smaller Fermi energy means less electrons are able to escape the magnetic confinement [$\phi_{\max}$ increases in Eq. (3)]. Since snakelike orbits can have a vanishingly small period $2\phi/\omega_c$, the coherence condition $2\phi/\omega_c \ll \tau$ is nearly always satisfied. We therefore interpret the persistence of ballistic effects long after the disappearance of Shubnikov–de Haas oscillations as further evidence in favor of magnetic edge states. The resistance minimum seen beyond the peak, in Fig. 4, results from the competition between two opposing effects. Increasing B_a increases the number of cycloidlike orbits but reduces their drift. At large applied fields $B_a \gg B_1^0, B_2^0$, these orbits cease drifting as cyclotron radii on both sides of the magnetic step become the same. The onset of the broad shoulder seen at ~400 mT in both experimental and theoretical curves occurs when cycloidlike edge states fill the whole Fermi surface ($\phi_2' = 0, \phi_1 = \pi$) and subsequently their number cannot increase any further.

The parallel drawn between Figs. 2 and 3 is a useful test of our model since Eq. (2) predicts both should be the same. Similarities in the peak position, the zero field resistance, and the sublinear behavior beyond the peak indicate that R_{xy} is controlled by the formation of magnetic edge states and is therefore no longer proportional to the average magnetic field in the cross-junction [18]. Further elaboration on our analytical model may require an exact solution to the full diffusive problem [1] as was already attempted for magnetic superlattices [19].

In summary, we have imposed a strong magnetic field gradient on 2D electrons and measured their conductivity along the drift path. A resistance resonance effect was observed at B_p due to two new types of magnetic edge states which arise at $B_a > B_p$ and $B_a < B_p$. The data are in good agreement with the drift-diffusion model of the system. The effect of magnetic edge states on the Hall resistance was demonstrated for the first time.

We gratefully acknowledge support from EPSRC (Grant No. GR/M67551), the Nuffield foundation, and the Royal Society (UK).

[1] C. W. J. Beenakker, Phys. Rev. Lett. **62**, 2020 (1989).
[2] R. R. Gerhardts, Phys. Rev. B **53**, 11 064 (1996).
[3] M. L. Leadbeater, C. L. Foden, J. H. Burroughes, M. Pepper, T. M. Burke, L. L. Wang, M. P. Grimshaw, and D. A. Ritchie, Phys. Rev. B **52**, R8629 (1995).
[4] P. D. Ye, D. Weiss, R. R. Gerhardts, M. Seeger, K. Von Klitzing, K. Eberl, and H. Nickel, Phys. Rev. Lett. **74**, 3013 (1995).
[5] M. Kato, A. Endo, S. Katsumoto, and Y. Iye, Phys. Rev. B **58**, 4876 (1998).
[6] V. Kubrak, F. Rahman, B. L. Gallagher, P. C. Main, M. Henini, C. H. Marrows, and M. A. Howson, Appl. Phys. Lett. **74**, 2507 (1999).
[7] H. A. Carmona, A. K. Geim, A. Nogaret, P. C. Main, T. J. Foster, M. Henini, S. P. Beaumont, and M. G. Blamire, Phys. Rev. Lett. **74**, 3009 (1995).
[8] P. D. Ye, D. Weiss, R. R. Gerhardts, G. Lutjering, K. von Klitzing, and H. Nickel, Semicond. Sci. Tech. **11**, 1613 (1996).
[9] J. H. Smet, K. von Klitzing, D. Weiss, and W. Wegscheider, Phys. Rev. Lett. **80**, 4538 (1998).
[10] A. Nogaret, S. Carlton, B. L. Gallagher, P. C. Main, M. Henini, R. Wirtz, R. Newbury, M. A. Howson, and S. P. Beaumont, Phys. Rev. B **55**, R16 037 (1997).
[11] J. E. Muller, Phys. Rev. Lett. **68**, 385 (1992).
[12] J. Reijniers, F. M. Peeters, and A. Matulis, Phys. Rev. B **59**, 2817 (1999).
[13] H. S. Sim, K. H. Ahn, K. J. Chang, G. Ihm, N. Kim, and S. J. Lee, Phys. Rev. Lett. **80**, 1501 (1998).
[14] The thermal expansion coefficients of Fe, Ni, and Ti/Au are identical to within 4%, whereas the mismatch with GaAs reaches 83%.
[15] Y. B. Xu, E. T. M. Kernohan, D. J. Freeland, A. Ercole, M. Tselepi, and A. C. Bland, Phys. Rev. B **58**, 890 (1998).
[16] D. Craik, *Magnetism: Principles and Applications* (John Wiley, Chichester, 1995).
[17] C. Kittel, *Introduction to Solid State Physics* (J. Wiley, New York, 1976), 5th ed.
[18] F. M. Peeters and X. Q. Li, Appl. Phys. Lett. **72**, 572 (1998).
[19] S. D. M. Zwerschke and R. R. Gerhardts, Physica (Amsterdam) **256B**, 28 (1998).